MODELING THE MOST LUMINOUS SUPERNOVA ASSOCIATED WITH A GAMMA-RAY BURST, SN 2011KL

Shan-Qin Wang 1,2,3 , Zach Cano 4 , Ling-Jun Wang 5 , WeiKang Zheng 3 , Zi-Gao Dai 1,2 , Alexei V. Filippenko 3,6 , and Liang-Duan Liu 1,2

¹School of Astronomy and Space Science, Nanjing University, Nanjing 210093, China; dzg@nju.edu.cn

²Key Laboratory of Modern Astronomy and Astrophysics (Nanjing University), Ministry of Education, China

³Department of Astronomy, University of California, Berkeley, CA 94720-3411, USA

⁴Instituto de Astrofísica de Andalucía (IAA-CSIC), Glorieta de la Astronomía s/n, E-18008, Granada, Spain

⁵Astroparticle Physics, Institute of High Energy Physics, Chinese Academy of Sciences, Beijing 100049, China and

⁶Miller Senior Fellow, Miller Institute for Basic Research in Science, University of California, Berkeley, CA 94720, USA

Draft version April 16, 2018

ABSTRACT

We study the most luminous known supernova (SN) associated with a gamma-ray burst (GRB), SN 2011kl. The photospheric velocity of SN 2011kl around peak brightness is $21,000 \pm 7,000$ km s⁻¹. Owing to different assumptions related to the light-curve (LC) evolution (broken or unbroken power-law function) of the optical afterglow of GRB 111209A, different techniques for the LC decomposition, and different methods (with or without a near-infrared contribution), three groups derived three different bolometric LCs for SN 2011kl. Previous studies have shown that the LCs without an early-time excess preferred a magnetar model, a magnetar+ 56 Ni model, or a white dwarf tidal disruption event model rather than the radioactive heating model. On the other hand, the LC shows an early-time excess and dip that cannot be reproduced by the aforementioned models, and hence the blue-supergiant model was proposed to explain it. Here, we reinvestigate the energy sources powering SN 2011kl. We find that the two LCs without the early-time excess of SN 2011kl can be explained by the magnetar+ 56 Ni model taking into account the cooling emission from the shock-heated envelope of the SN progenitor, demonstrating that this SN might primarily be powered by a nascent magnetar.

Subject headings: stars: magnetars — supernovae: general — supernovae: individual (SN 2011kl)

1. INTRODUCTION

The optical spectra of Type Ic supernovae (SNe Ic) lack hydrogen and helium absorption lines (see, e.g., Filippenko 1997; Matheson et al. 2001 for reviews). A small fraction of SNe Ic have spectra with broad absorption troughs indicating large photospheric velocities and were dubbed "broad-lined SNe Ic (SNe Ic-BL)" (Woosley & Bloom 2006). Some SNe Ic-BL have very large kinetic energies ($\gtrsim 10^{52}$ erg; e.g., Iwamoto et al. 1998; Mazzali et al. 2000, 2002, 2005; Valenti et al. 2008) and were coined "hypernovae" (Iwamoto et al. 1998). Hypernovae are usually rather luminous (with peak luminosities $\sim 10^{43} \text{ erg s}^{-1}$), indicating that they must have synthesized ~ 0.5 M_{\odot} of ^{56}Ni if they can be explained by the radioactive heating model (Arnett 1982; Cappellaro et al. 1997; Valenti et al. 2008; Chatzopoulos et al. 2012). Moreover, some SNe Ic-BL are associated with longduration gamma-ray bursts (GRBs; e.g., Galama et al. 1998; Stanek et al. 2003; Hjorth et al. 2003) and have been called "GRB-SNe" (see Woosley & Bloom 2006; Hjorth & Bloom 2012; Cano et al. 2017, and references therein). While most GRB-SNe are Type Ic-BL, not all SNe Ic-BL are associated with GRBs. The most luminous SNe Ic are Type Ic superluminous supernovae (SLSNe; Quimby et al. 2011; Gal-Yam 2012); their peak luminosities are $\gtrsim 7 \times 10^{43} \ \rm erg \ s^{-1}$ (Gal-Yam 2012), tens of times greater than those of ordinary SNe.

In this paper, we study a very luminous SN Ic, SN 2011kl, which is associated with an ultralong ($T_{90} \approx$

10⁴ s) GRB 111209A (see, e.g., Palmer et al. 2011; Golenetskii et al. 2011; Gendre et al. 2013; Stratta et al. 2013; Gompertz & Fruchter 2017) at redshift z=0.677 (Vreeswijk et al. 2011). By using WMAP ΛCDM cosmology (Spergel et al. 2003) and adopting $H_0=71~{\rm km~s^{-1}~Mpc^{-1}}$, $\Omega_M=0.27$, and $\Omega_{\Lambda}=0.73$, Kann et al. (2016) derived a luminosity distance (D_L) of 4076.5 Mpc for GRB 111209A/SN 2011kl. With a peak luminosity $\sim 3.63^{+0.17}_{-0.16} \times 10^{43}~{\rm erg~s^{-1}}$ (Kann et al. 2016)¹, SN 2011kl is the most luminous GRB-SN yet detected and is significantly more luminous than all other GRB-SNe, whose average peak luminosity is $1 \times 10^{43}~{\rm erg~s^{-1}}$ with a standard deviation of $0.4 \times 10^{43}~{\rm erg~s^{-1}}$ (Cano et al. 2017). The time of peak brightness of SN 2011kl is $\sim 14~{\rm days}$, slightly larger than the average (13.0 days with a standard deviation of 2.7 days; Cano et al. 2017) of other GRB-SNe.

The peak luminosity of SN 2011kl is comparable to that of some not-quite-superluminous "SLSNe" (e.g., PTF11rks, PTF10hgi, iPTF15esb, iPTF16bad, and PS15br) and commensurate with the SN-SLSN gap transients observed by Arcavi et al. (2016); moreover, Liu et al. (2017c) pointed out that the spectrum of SN 2011kl is very different from those of GRB-SNe, but consistent with that of SLSNe. So, the energy sources powering its LC might be similar to those powering the SLSN LCs instead of the or-

 $^{^{1}}$ Greiner et al. (2015) found a slightly lower peak luminosity ($\sim 2.8^{+1.2}_{-1.0} \times 10^{43}~{\rm erg~s^{-1}})$ since they ignored the near-infrared contribution

dinary SNe Ic. The most popular prevailing models for explaining SLSNe are the magnetar model (Maeda et al. 2007; Kasen & Bildsten 2010; Woosley 2010; Chatzopoulos et al. 2012, 2013; Inserra et al. 2013; Chen et al. 2015; Wang et al. 2015a, 2016b; Dai et al. 2016; Moriya et al. 2017) and the ejecta plus circumstellar medium (CSM) interaction model (Chevalier 1982; Chevalier & Fransson 1994; Chugai & Danziger 1994; Chatzopoulos et al. 2012, 2013; Liu et al. 2017a).

There have been several papers modeling the LCs of SN 2011kl. The LC obtained by Greiner et al. (2015) (hereafter the G15 LC) cannot be explained by the ⁵⁶Ni model but can be by the magnetar model (Greiner et al. 2015; Cano et al. 2016) ³, the magnetar+⁵⁶Ni model (Metzger et al. 2015; Bersten et al. 2016), the white dwarf tidal disruption event (WD TDE) model (Ioka et al. 2016), and the collapsar model (Gao et al. 2016) involving a stellar-mass black hole and a fallback accretion disk (Woosley 1993; MacFadyen & Woosley By subtracting the contribution from the ultraviolet (UV)/optical/near-infrared (NIR) afterglow (Kann et al. 2017) of GRB 111209A, Kann et al. (2016) obtained a new bolometric LC (hereafter the K16 LC) and modeled it with the radioactive heating model, finding $2.27\pm0.64~{\rm M}_{\odot}$ of $^{56}{\rm Ni}$ and $6.79^{+3.67}_{-2.84}~{\rm M}_{\odot}$ of ejecta, suggesting that this model is disfavored. The LC derived by Ioka et al. (2016) (hereafter the I16 LC) has an early-time excess and a dip 4 which cannot be reproduced by the models mentioned above, but it can be fit by the blue supergiant (BSG) model with explosive energy injection ("the BSG model"; Kashiyama et al. 2013; Nakauchi et al. 2013; Ioka et al. 2016). However, it is premature to exclude the magnetar model in explaining the I16 LC since the cooling emission from the shockheated extended envelope (Piro 2015) or the emission from magnetar shock breakout (Kasen et al. 2016) can reproduce the early-time excess.

Thus, the issue of the energy source of SN 2011kl deserves additional attention. In this paper, we reinvestigate the possible mechanisms powering the LC of SN 2011kl and discuss their implications. In Section 2, we use the radioactive heating model, the magnetar model, the magnetar+ 56 Ni model, and the magnetar+ 56 Ni+cooling model to fit the LCs of SN 2011kl. Our discussion and conclusions are presented in Sections 3 and 4, respectively.

2. MODELING THE LIGHT CURVES OF SN 2011KL

 2 Almost all SLSNe (except maybe pair-instability SLSNe — e.g., SN 2007bi Gal-Yam et al. 2009; but see Dessart et al. 2012 and Nicholl et al. 2013) cannot be explained by the radioactive heating model (Quimby et al. 2011; Inserra et al. 2013; Nicholl et al. 2013, 2014). Some SLSNe I exhibiting late-time rebrightening and ${\rm H}\alpha$ emission lines (Yan et al. 2015, 2017) might be powered by a hybrid model containing contributions from magnetars and ejecta-CSM interaction (Wang et al. 2016c).

 3 Cano et al. (2016) showed that GRB 111209A and SN 2011kl can be explained purely by the magnetar model, both for the afterglow and SN-powered phases.

This early-time excess arose from the assumption that a single power law could describe the evolution of the optical LC during the afterglow phase. A broken power law showed no such excess (e.g., Greiner et al. 2015; Kann et al. 2016), so this excess is model-dependent. Moreover, a single power law was used by Cano et al. (2016), and no such excess was observed, making it inconclusive.

Extracting the LC of a SN associated with a GRB is difficult since this process requires a decomposition of the observations to account for the contributions from the optical afterglow, the SN, and the underlying host galaxy (e.g., Zeh et al. 2004); moreover, it depends on the assumptions adopted for modeling the GRB optical afterglow. By assuming that the LC of the optical afterglow of GRB 111209A can be described by a broken power-law function and subtracting the contributions from the optical afterglow and the host galaxy, Greiner et al. (2015) obtained the LC of SN 2011kl (the G15 LC). The G15 LC did not include the NIR contribution and is a pseudobolometric LC. By adding the NIR contribution, Kann et al. (2016) obtained a genuine bolometric LC (the K16 LC)⁵. However, based on the assumption that the optical afterglow of GRB 111209A can also be described by a single (unbroken) power-law function, Ioka et al. (2016) derived another LC (the I16 LC) for SN 2011kl. This LC has an early-time excess and a dip. Hence, SN 2011kl has three different LCs (see Figure 1) that must be modeled.

The LCs of SLSNe PTF11rks and PTF10hgi (Inserra et al. 2013) are also plotted in Figure 1. By comparing the K16 LC of GRB-SN 2011kl, whose peak luminosity $L_{\rm peak,bol}$ is $\sim 3.6 \times 10^{43}$ erg s⁻¹, to the LCs of SLSNe PTF11rks and PTF10hgi, we find that the peak of the LC of SN 2011kl is as luminous as that of these two SLSNe. Furthermore, we point out that other SLSNe also have similar values of $L_{\rm peak,bol}$ — e.g., iPTF15esb ($L_{\rm peak,bol} \approx 4 \times 10^{43}$ erg s⁻¹; Yan et al. 2017), iPTF16bad ($L_{\rm peak,bol} \approx 4 \times 10^{43}$ erg s⁻¹; Yan et al. 2017), and PS15br ($L_{\rm peak,bol} \approx 4.15 \times 10^{43}$ erg s⁻¹; Inserra et al. 2016).

In this section, we use some models to fit these LCs. For the G15 and K16 LCs, we adopt the Markov Chain Monte Carlo (MCMC) method to minimize the values of χ^2 /dof and get the best-fit parameters and the range. For the I16 LC, we don't use the MCMC method because its data have no known error bars.

2.1. The Radioactive Heating Model

Based on their derived LC (the G15 LC), Greiner et al. (2015) fit the $^{56}{\rm Ni}$ model and found that the required mass of $^{56}{\rm Ni}$ is $\sim 1~{\rm M}_{\odot}$ if the LC was powered by $^{56}{\rm Ni}$ decay. Kann et al. (2016) suggested that their bolometric LC (the K16 LC), which included the NIR contribution, needed $2.27\pm0.64~{\rm M}_{\odot}$ of $^{56}{\rm Ni}$ to reproduce its luminosity if the LC was powered by radioactive heating.

Here we employ the semi-analytic 56 Ni model (Arnett 1982; Cappellaro et al. 1997; Valenti et al. 2008; Chatzopoulos et al. 2012) to repeat the fits for the G15 LC, the K16 LC and I16LC. The free parameters of the 56 Ni model are the optical opacity κ , the ejecta mass $M_{\rm ej}$, the 56 Ni mass $M_{\rm Ni}$, the initial scale velocity

 6 SN 2011kl, along with PTF11rks, PTF10hgi, iPTF15esb, iPTF16bad, and PS15br, are dimmer than the strict threshold for SLSNe ($L_{\rm peak} > 7 \times 10^{43} \ {\rm erg \ s^{-1}}$ and the peak absolute magnitudes $M_{\rm peak} < -21 \ {\rm mag} \ in \ any \ band;$ Gal-Yam 2012).

 $^{^5}$ The K16 LC must be brighter than the pseudobolometric LC (the G15 LC) without the NIR contribution. However, the median values of the luminosities of the first two points of the K16 LC are dimmer than that of the G15 LC. This fact is puzzling, perhaps indicating that the uncertainties are rather large.

of the ejecta⁷ $v_{\rm sc0}$, and the gamma-ray opacity of ⁵⁶Nicascade-decay photons $\kappa_{\gamma,Ni}$. The value of κ is rather uncertain and has been assumed to be 0.06 cm² g⁻¹ (e.g., Valenti et al. 2011; Lyman et al. 2016), 0.07 cm^2 g^{-1} (e.g., Chugai 2000; Taddia et al. 2015; Wang et al. 2015b), 0.07 ± 0.01 cm² g⁻¹ (e.g., Greiner et al. 2015; Kann et al. 2016), 0.08 cm² g⁻¹ (e.g., Arnett 1982; Mazzali et al. 2000), $0.10 \text{ cm}^2 \text{ g}^{-1}$ (e.g., Inserra et al. 2013; Wheeler et al. 2015), and $0.20 \text{ cm}^2 \text{ g}^{-1}$ (e.g., Kasen & Bildsten 2010; Nicholl et al. 2014; Arcavi et al. 2016). Assuming that the dominant opacity source is Thomson electron scattering and the temperature of the SN ejecta consisting of carbon and oxygen is not very high ($\lesssim 10,000$ K), we adopted 0.07 cm² g⁻¹ to be the value of κ . The value of $\kappa_{\gamma,\rm Ni}$ is fixed to be 0.027 cm² g^{-1} (e.g., Cappellaro et al. 1997; Mazzali et al. 2000; Maeda et al. 2003; Wheeler et al. 2015). The photospheric velocity of SN 2011kl inferred from the spectra is $\sim 21,000 \pm 7,000 \text{ km s}^{-1}$ (Kann et al. 2016). We assume that the moment of explosion (t_{expl}) for SN 2011kl is equal to that of GRB 111209A.

The LCs reproduced by the radioactive heating models A1, A2, and A3 are shown in Figure 2, and the best-fit parameters are listed in Table 1. While the best-fit model parameters for the G15 LC are approximately equal to that derived by Greiner et al. (2015), our inferred $^{56}\rm Ni$ mass $(1.42^{+0.04}_{-0.04}~\rm M_{\odot})$ for the K16 LC is smaller than the value derived by Kann et al. (2016) $(2.27\pm0.64~\rm M_{\odot}).$ Moreover, the value of the ejecta mass $(4.57^{+0.80}_{-1.03}~\rm M_{\odot})$ is also smaller than that derived by Kann et al. (2016) $(6.79^{+3.67}_{-2.84}~\rm M_{\odot}).$

Another method for estimating the value of ⁵⁶Ni is to use the "Arnett law" (Arnett 1982), which says that the ⁵⁶Ni energy input LC intersects the peak of the SN LC. According to the Arnett law and Eq. 19 of (Nadyozhin 1994), the mass of ⁵⁶Ni is ⁸

$$M_{\text{Ni}} = (L_{\text{peak}}/10^{43} \text{ erg s}^{-1})[6.45 \ e^{-t_{\text{rise}}/8.8 \text{ days}}]$$

 $+1.45 \ e^{-t_{\text{rise}}/111.3 \text{ days}}]^{-1} \ \text{M}_{\odot}, \quad (1)$

since the value of $t_{\rm rise}$ of SN 2011kl is ~ 14 days and the peak luminosity is $3.63^{+0.17}_{-0.16} \times 10^{43}$ erg s⁻¹ (for the K16 LC) or $2.8^{+1.2}_{-1.0} \times 10^{43}$ erg s⁻¹ (for the G15 LC), the 56 Ni mass is $1.40^{+0.07}_{-0.06}$ M $_{\odot}$ (for the K16 LC) or $1.08^{+0.46}_{-0.39}$ M $_{\odot}$ (for the G15 LC).

2.2. The Magnetar Model

Greiner et al. (2015) analyzed the spectrum of SN 2011kl and pointed out that the spectral features imply that the 56 Ni mass must be significantly smaller than 1 M_{\odot} ; they excluded the 56 Ni model for explaining the LC of SN 2011kl. Alternatively, Greiner et al.

(2015) employed the magnetar model developed by Kasen & Bildsten (2010) to fit the G15 LC and obtained a rather good result. But the K16 LC has not yet been fit with the magnetar model.

Here, we use the semianalytic magnetar model developed by Wang et al. (2015a) and Wang et al. (2016b) that considers the leakage, photospheric recession, and acceleration effects to fit the K16 LC, and we repeat the fits for the G15 LC. The free parameters of the magnetar model are κ , $M_{\rm ej}$, the magnetic strength of the magnetar B_p , the initial rotation period of the magnetar P_0 , $v_{\rm sc0}$, and the gamma-ray opacity of magnetar photons $\kappa_{\gamma,\rm mag}$. The value of $\kappa_{\gamma,\rm mag}$ depends mainly on the energy of the photons ($E_{\rm photons}$) emitted from the nascent magnetars, varying between ~ 0.01 and $0.2~{\rm cm^2~g^{-1}}$ for γ -ray photons ($E_{\gamma} \gtrsim 10^6~{\rm eV}$) and between $\sim 0.2~{\rm and}~10^4~{\rm cm^2~g^{-1}}$ for X-ray photons ($10^2~{\rm eV} \lesssim E_{\rm X} \lesssim 10^6~{\rm eV}$); see Fig. 8 of Kotera et al. (2013).

The LCs reproduced by the magnetar models (B1, B2, and B3) are shown in Figure 2 and the best-fit parameters are listed in Table 1. We find that the K16 LC can be powered by a magnetar having $B_p = 5.99^{+1.75}_{-5.55} \times 10^{14}$ G and $P_0 = 10.83^{+0.49}_{-6.94}$ ms, while the G15 LC can be powered by a magnetar with $B_p = 9.72^{+3.23}_{-4.13} \times 10^{14}$ G and $P_0 = 12.07^{+1.15}_{-2.52}$ ms (the values of B_p and P_0 derived by Greiner et al. (2015) are $\sim (6-9) \times 10^{14}$ G and ~ 13.4 ms, respectively).

2.3. The Magnetar Plus ⁵⁶Ni Model

The contribution of 56 Ni cannot be ignored when modeling some luminous SNe Ic (Wang et al. 2015b; Metzger et al. 2015; Bersten et al. 2016). Wang et al. (2015b) instead used a hybrid model containing contributions from 56 Ni and a magnetar to fit three luminous SNe Ic-BL whose peak luminosities are approximately equal to that of SN 2011kl. Metzger et al. (2015) and Bersten et al. (2016) used the same model to fit SN 2011kl, suggesting that $0.2 \,\mathrm{M}_{\odot}$ of 56 Ni must be added so that a better fit can be obtained. Therefore, we used the hybrid model (the 56 Ni+magnetar model) to fit the K16 LC and the G15 LC. The free parameters of this model are κ , M_{ei} , M_{Ni} , B_{D} , P_{O} , v_{SCO} , κ_{NNi} , and $\kappa_{\mathrm{N,mag}}$.

model are κ , $M_{\rm ej}$, $M_{\rm Ni}$, B_p , P_0 , $v_{\rm sc0}$, $\kappa_{\gamma,\rm Ni}$, and $\kappa_{\gamma,\rm mag}$. Since an energetic SN explosion can synthesize ~ 0.2 ${\rm M}_{\odot}$ of $^{56}{\rm Ni}$ (Nomoto et al. 2013; Maeda & Tominaga 2009), we assumed that the range of $^{56}{\rm Ni}$ is 0-0.2 ${\rm M}_{\odot}$ (for the G15 and K16 LCs with error bars, which allow us to use the MCMC method and determine the best-fit parameters) or 0.2 ${\rm M}_{\odot}$ (for the I16 LC without error bars). The LCs reproduced by the 56 Ni+magnetar model (C1, C2, and C3) are shown in Figure 2 and the best-fit parameters are listed in Table 1. We find that this hybrid model can also reproduce good fits, and that almost all parameters (except for P_0) adopted by the $^{56}{\rm Ni+magnetar}$ model are the same as that of the magnetar models. Moreover, the masses of $^{56}{\rm Ni}$ determined by the MCMC are $0.11^{+0.06}_{-0.07}$ ${\rm M}_{\odot}$ (for the K16 LC) and $0.10^{+0.06}_{-0.07}$ ${\rm M}_{\odot}$ (for the G16 LC).

2.4. The magnetar plus ⁵⁶Ni plus cooling model

The I16 LC has an early-time excess which cannot be reproduced by the $^{56}{\rm Ni}$ model, the magnetar model,

 $^{^7}$ The scale velocity of the ejecta $v_{\rm sc}$ is the velocity of the surface of the ejecta. The radius of the ejecta can be calculated from $R(t)=R(0)+v_{\rm sc}t$ (Arnett 1982).

 $^{^8}$ Eq. 19 of Nadyozhin (1994) is valid only in the case of full gamma-ray trapping. For partial gamma-ray trapping ($\kappa_{\gamma,\mathrm{Ni}} = 0.027~\mathrm{cm}^2~\mathrm{g}^{-1}$), however, the inferred 56 Ni mass is equal to that corresponding to the case of full gamma-ray trapping, because the gamma-ray leakage doesn't influence the luminosity before and around the LC peak.

or the magnetar+⁵⁶Ni model (A3, B3, and C3, respectively; see Figure 2). The WD-TDE model proposed by Ioka et al. (2016) also cannot explain the I16 LC (see Figure 1 of Ioka et al. 2016). Ioka et al. (2016) suggested that the I16 LC can be explained by the BSG model.

Here, we use another model to explain the I16 LC. We suggest that the early-time excess might be due to the cooling emission from the shock-heated extended envelope (Nakar & Piro 2014; Piro 2015), while the main peak of the LC might be powered by a magnetar or a magnetar plus a moderate amount of $^{56}{\rm Ni}$. In this scenario, the progenitor of the SN is surrounded by an extended, low-mass envelope which is heated by the SN shock and produces a declining bolometric LC when it cools. At the same time, sources at the center of the SN release energy and produce a rising LC until it peaks. By combining the magnetar($+^{56}$ Ni) model developed by Wang et al. (2015b) and Wang et al. (2016b) and the cooling model developed by Piro (2015), a LC with an early-time excess and a dip can be produced. In this model, two additional parameters must be added: the mass of the extended envelope $(M_{\rm env})$ and the radius of the extended envelope $(R_{\rm env})$.

The LCs reproduced by the cooling modeland the magnetar+ 56 Ni+cooling model (D1–D3) are shown in Figure 2 and the corresponding parameters are listed in Table 1. We find that the magnetar+ 56 Ni+cooling models (D2 and D3) can well fit the entire I16 LC. In the scenario containing the contribution from the cooling emission, the progenitor of SN 2011kl was supposed to be surrounded by an extended envelope whose mass and radius are $\sim 0.63~{\rm M}_{\odot}$ (or $\sim 0.45~{\rm M}_{\odot}$) and $\sim 51.4~{\rm R}_{\odot}$ (or $\sim 103~{\rm R}_{\odot}$), respectively. Owing to the parameter degeneracy, there must be other choices of these two parameters.

One advantage of the magnetar-dominated model is that it can explain the I16 LC if the cooling emission from the extended envelope is added, and it can explain the K16 LC and the G15 LC if the progenitor was not surrounded by an extended envelope. Another advantage is that the LC reproduced by the model with cooling emission can trace the entire LC (including the early excess, the dip, the peak, and the post-peak) while the LC reproduced by the BSG model is a smooth, monotonically decreasing LC that is brighter than the dip and dimmer than the peak. Although the uncertainties of the early-time data indicate that the LC reproduced by the BSG model might fit the data, the magnetar+ 56 Ni+cooling model can give a better match.

$2.5. \ Summary$

In summary, the K16, G15, and I16 LCs cannot be powered solely by the $^{56}{\rm Ni}$ model since (a) $\sim 1.00-1.42$ ${\rm M}_{\odot}$ of $^{56}{\rm Ni}$ is inconsistent with the spectral analysis performed by Greiner et al. (2015), and (b) the ratio of $^{56}{\rm Ni}$ masses ($\sim 1.0-1.4~{\rm M}_{\odot}$) to the ejecta mass ($\sim 2-5~{\rm M}_{\odot}$) is ~ 0.3 , which is significantly larger than the upper limit (~ 0.20 ; Umeda & Nomoto 2008). Alternatively, the K16 and G15 LCs can be explained by the magnetar

model and the ⁵⁶Ni+magnetar model; the values of $M_{\rm ej}$, B_p , and P_0 can be found in Table 1.

Owing to the degeneracy of model parameters, the values of these parameters have many choices that can also give the best-fit LC. For example, Bersten et al. (2016) obtained $P_0=3.5$ ms, $B_p=1.95\times 10^{15}$ G, $M_{\rm ej}=2.5$ M $_{\odot}$ if $\kappa=0.2$ cm 2 g $^{-1}$, and $M_{\rm Ni}=0.2$ M $_{\odot}$; Metzger et al. (2015) derived $P_0\approx 2$ ms, $B_p\approx 4\times 10^{14}$ G, $M_{\rm ej}=3$ M $_{\odot}$ if $\kappa=0.2$ cm 2 g $^{-1}$, and $M_{\rm Ni}=0.2$ M $_{\odot}$; and Cano et al. (2016) derived $P_0=11.5$ –13.0 ms, $B_p=(1.1$ –1.3) $\times 10^{15}$ G, and $M_{\rm ej}=5.2$ M $_{\odot}$ if $\kappa=0.07$ cm 2 g $^{-1}$.

3. DISCUSSION

3.1. What Determines the Peak Luminosities of SNe and SLSNe?

The inferred best-fit values of P_0 and B_p of the magnetar powering the LCs of SN 2011kl are ~ 9 –14 ms and $\sim (6$ –14) $\times 10^{14}$ G, respectively. The values of P_0 obtained by Bersten et al. (2016), Metzger et al. (2015), and Cano et al. (2016) are 3.5 ms, 2 ms, and 11.5–13.0 ms (respectively), while the respective values of B_p derived by these groups are 1.95×10^{15} G, $\sim 4\times 10^{14}$ G, and $(1.1-1.3)\times 10^{15}$ G. The spin-down timescale of a magnetar (τ_p) is determined by the values of P_0 and B_p , $\tau_p = 1.3 \, (B_p/10^{14} \text{ G})^{-2} (P_0/10 \text{ ms})^2 \text{ yr}$ (Kasen & Bildsten 2010). We note that other SLSNe Ic whose peak luminosities are larger than $\sim 10^{44}~{\rm erg~s^{-1}}$ must be powered by magnetars with $P_0 \approx 1\text{--}10$ ms and $10^{13}\text{--}10^{15}$ (see, e.g., Inserra et al. 2013; Nicholl et al. 2014; Liu et al. 2017b; Nicholl et al. 2017; Yu et al. 2017), indicating that the values of P_0 and B_p play a crucial role in determining the peak luminosities of SLSNe. When $P_0 \gtrsim 10 \text{ ms}$ and B_p is a few 10^{14} G , the magnetarpowered SNe are luminous (Wang et al. 2015b); when $P_0 \lesssim 10 \text{ ms}$ and B_p is a few 10^{16} G , the magnetars can explain the LCs of some SNe Ic-BL (Wang et al. 2016a, 2017a,b; see also Chen et al. 2017), while Cano et al. (2016) suggested that most GRB-SNe are powered by radioactive heating.

Wang et al. (2015b) emphasized the role of P_0 while Yu et al. (2017) highlighted the role of B_p . We suggest that the more reasonable scheme discussing the factors influencing the peak luminosities and the shapes of magnetar-powered SNe and SLSNe is to take into account both of these parameters. However, it should be noted that the values of τ_m (or $M_{\rm ej}$) also influence the peak luminosities of magnetar-powered SNe and SLSNe (Nicholl et al. 2015). Hence, the luminosities of SNe and SLSNe are determined by all of these parameters (P_0 , P_p , and P_m , which is primarily determined by P_m and cannot solely be influenced by any single one. Similarly, the peak luminosities of SNi-powered SNe and SLSNe are determined by the values of P_m and P_m .

3.2. Correlations Between the Opacity and Other Parameters

In Section 2, we assumed that the value of κ is 0.07 cm² g⁻¹. As mentioned above, however, the value of κ is rather uncertain (0.06–0.20 cm² g⁻¹). Therefore, it is necessary to explore the correlations between the opacity and all other parameters involved in the modeling.

 $^{^9}$ The energy of the SN, $E_{\rm SN},$ must also be added into the modeling. However, it can be supposed that $E_{\rm SN}=E_{\rm K}=0.3\,M_{\rm ej}v_{\rm sc}^2,$ so this parameter is determined by $M_{\rm ej}$ and $v_{\rm sc},$ while $v_{\rm sc}$ is determined by $v_{\rm sc0},\,B_p,$ and P_0 (the acceleration effect).

Assuming $\kappa = 0.10$ cm² g⁻¹ and 0.20 cm² g⁻¹, and using the ⁵⁶Ni model, the magnetar model, and the magnetar plus ⁵⁶Ni model, we repeated the fits for the K16 LC and the G15 LC, obtaining the best-fit parameters (see Table 1).

By comparing the values of the parameters corresponding to different values for κ , we found that while the values of the ejecta masses are significantly influenced by the values of κ and $M_{\rm ej} = a\kappa^{-1} + b$ (a and b are constants; see Figure 3, and a similar figure can be found in Nagy & Vinkó 2016), all other parameters are slightly affected by the values of κ and no correlation between them and κ has been found.

We did not study the correlations between the opacity and other parameters for the I16 LC, since its data lack error bars, and the value of $M_{\rm ej}$ is proportional to that of κ^{-1} while the values of all other parameters are completely independent of that of $M_{\rm ej}$.

3.3. The Initial Kinetic Energy of SN 2011kl

The multidimensional simulations (see Janka et al. 2016, and references therein) for neutrino-driven SNe suggest that the value of $E_{\rm K}$ provided by the neutrinos can be up to $\sim (2.0\text{--}2.5) \times 10^{51}$ erg. Provided the value of $v_{\rm sc0}$ is 14,000 km s⁻¹ (then the ejecta mass is lowered to 2.4 M $_{\odot}$ for the K16 LC or 1.4 M $_{\odot}$ for the I16 LC), the origin of $E_{\rm K,0}$ of SN 2011kl ($E_{\rm K,0}=0.3~M_{\rm ej}v_{\rm sc0}^2\approx 2.4\times 10^{51}$ erg) can be comfortably explained by the neutrino-driven model and other processes are not required to provide additional $E_{\rm K,0}$.

According to the equation $E_{\rm rot,0}\approx (1/2)I\Omega_0^2\approx 2\times 10^{52}\,(P_0/1~{\rm ms})^{-2}$ erg $(I\approx 10^{45}~{\rm g~cm}^2$ is the rotational inertia of the magnetar), we find that the initial rotational energy of the magnetar $(P_0=11.4\text{--}14.2~{\rm ms})$ powering the LCs of SN 2011kl is $\sim 1.5\times 10^{50}$ erg (Cano et al. 2016 obtained $E_{\rm rot,0}=(1.2\text{--}1.6)\times 10^{50}$ erg), significantly smaller than their $E_{\rm K,0}$. Even if the initial rotational energy of this magnetar is all converted to the $E_{\rm K,0}$ of the ejecta, the ratio of final $E_{\rm K}$ to $E_{\rm K,0}$ is ~ 1.1 . Therefore, the acceleration effect is rather small and can be neglected.

3.4. The Ejecta Mass and Binarity

Assuming that $\kappa=0.07~\rm cm^2~g^{-1}$ and according to the results of our work based on the magnetar models (the $^{56}\rm Ni$ models have been excluded), the inferred ejecta mass of SN 2011kl is $3.83^{+2.06}_{-1.46}~\rm M_{\odot}$ (for the K16 LC), $4.76^{+3.05}_{-1.78}~\rm M_{\odot}$ (for the G15 LC), or $\sim2.12~\rm M_{\odot}$ (for the I16 LC). If $\kappa=0.10~\rm cm^2~g^{-1}$ or $0.20~\rm cm^2~g^{-1}$ were adopted, the inferred masses would decrease by a factor of about $2\text{--}3,\,\sim1\text{--}2~\rm M_{\odot}$.

By adopting $\kappa = 0.04$ cm² g⁻¹ and v ($v_{\rm sc0}$) = 20,000 km s⁻¹, Ioka et al. (2016) concluded that the mass of the ejecta is 2 M $_{\odot}$ if SN 2011kl is powered by a magnetar. Assuming that $\kappa = 0.07$ cm² g⁻¹ and v ($v_{\rm sc0}$) = 21,000 km s⁻¹, the ejecta mass must be 2 M $_{\odot}$ × 0.04/0.07 × 21,000/20,000 = 1.323 M $_{\odot}$, significantly smaller than the value derived here (2.12 M $_{\odot}$).

This difference is caused by the fact that we adopted the equation $\tau_m = (2\kappa M_{\rm ej}/\beta v_{\rm sc}c)^{1/2}$ while Ioka et al. (2016) adopted the equation $\tau_m = (3\kappa M_{\rm ej}/4\pi v_{\rm sc}c)^{1/2}$.

The ratio of the masses derived from these two equations is $3\beta/8\pi = 3 \times 13.8/8 \times 3.1416 = 1.647$. By multiplying this factor by 1.323 $\rm M_{\odot}$, we obtain 2.18 $\rm M_{\odot}$, consistent with the value derived here (2.12 $\rm M_{\odot}$). The ejecta mass would be 1.45 $\rm M_{\odot}$ if $\kappa = 0.1~\rm cm^2~\rm g^{-1}$ and $\tau_m = (2\kappa M_{\rm ej}/\beta v_{\rm sc}c)^{1/2}$.

Ioka et al. (2016) and Arcavi et al. (2016) argued that the ejecta mass of SN 2011kl inferred from the magnetar model is too low to be produced by a core-collapse SN whose remnant harbors a magnetar. However, it must be pointed out that such a small value is not disfavored by the explosion of a SN Ic and magnetar formation, since the massive hydrogen and helium envelopes of the progenitors of SNe Ic had been stripped by their companions or winds, and the mean value of the ejecta mass of SNe Ic is $2.9~{\rm M}_{\odot}$ with a standard deviation of $2.2~{\rm M}_{\odot}$ (see Table 6 of Lyman et al. 2016). The inferred ejecta masses of Type Ic-BL SNe 2002ap, 2006aj, 2009bb, and 2010bh are $2.0^{+0.8}_{-0.7}\,\mathrm{M}_{\odot}$, $1.4^{+0.4}_{-0.2}\,\mathrm{M}_{\odot}$, $1.9^{+0.6}_{-0.5}\,\mathrm{M}_{\odot}$, and $0.9^{+0.2}_{-0.2}\,\mathrm{M}_{\odot}$, respectively (see Table 5 of Lyman et al. 2016). Note, especially, that SN 2006aj with $M_{\rm ej} = 1.4^{+0.4}_{-0.2}~{\rm M}_{\odot}$ (or ~ 2 M_{\odot} ; Mazzali et al. 2006) is a SN Ic-BL associated with an X-ray flash (a "soft GRB") that has long been believed to be powered by a nascent magnetar (Mazzali et al.

Such small ejecta masses indicate that the progenitor of SN 2011kl might be located in a binary system and most of its mass had been stripped by its companion before the explosion. Although the mass-transfer process reduced the mass of the progenitor, it can enhance the angular momentum and angular velocity of the progenitor, making it easier for the nascent neutron stars left by the SN explosions to be millisecond ($P_0 \approx 1$ –10 ms) magnetars.

4. CONCLUSIONS

In this paper, we modeled the LCs of SN 2011kl, which is the most luminous ($L_{\rm peak}=3.63^{+0.17}_{-0.16}\times10^{43}~{\rm erg~s^{-1}})$ GRB-SN identified thus far. By using the bolometric LC of SN 2011kl derived by Kann et al. (2016) and assuming that this SN is powered by $^{56}{\rm Ni}$ cascade decay, we find that the required $^{56}{\rm Ni}$ mass is $1.42^{+0.04}_{-0.04}~{\rm M}_{\odot}$, which is smaller than that (2.27 \pm 0.64 ${\rm M}_{\odot}$) inferred by Kann et al. (2016). The $^{56}{\rm Ni}$ model can be excluded from explaining the LCs of SN 2011kl, since the spectral features indicate that the amount of $^{56}{\rm Ni}$ must be significantly smaller than $\sim 1~{\rm M}_{\odot}$ (Greiner et al. 2015).

Alternatively, we used the magnetar model and the magnetar+⁵⁶Ni model to fit the K16 LC and the G15 LC, finding that both of the models can well explain these LCs. It is noteworthy that Ioka et al. (2016) argue that the fact that the location of GRB 111209A-SN 2011kl is near the nucleus of the host galaxy favors the WD-TDE model. However, the position of the SN does not necessarily mean that this event must be a TDE rather than a SN. The magnetar model is still possible, explaining the K16 LC and the G15 LC, while the TDE model is also a plausible one for the G15 LC and the K16 LC.

Whereas the magnetar model and the magnetar+⁵⁶Ni model can account for the K16 LC and the G15 LC, they cannot explain the I16 LC because these models cannot produce the early-time excess and the dip, although

the presence of the early-time excess is entirely modeldependent (i.e., the parameters of the optical-afterglow component in the LC decomposition technique). To solve this problem, we added the contribution of the cooling emission from a low-mass $(M_{\rm env} \approx 0.5 {\rm M}_{\odot})$, extended ($R_{\rm env} \approx 50\text{--}100 \text{ R}_{\odot}$) SN progenitor envelope, and found that the magnetar+cooling model and the magnetar+⁵⁶Ni+cooling model can account for the I16 LC. In these models, cooling emission from the shockheated envelope powers the early-time excess, while the magnetar or magnetar+56Ni power the main peak of the LC, and the sum of these two produces the dip. ¹⁰ Hence, we conclude that the BSG model is not unique for explaining the I16 LC even if the LC of SN 2011kl has an early-time excess, since a progenitor surrounded by a low-mass, extended envelope can also power a LC with an early excess.

It seems that the magnetar+ 56 Ni+cooling and the magnetar+ 56 Ni models are more reasonable than the magnetar and magnetar+cooling models for the LCs of SN 2011kl, since core-collapse SNe must synthesize a moderate amount of 56 Ni. However, discriminating between the LCs reproduced by the models with and without 56 Ni is very difficult because the contribution of a moderate amount of 56 Ni ($\sim 0.1-0.2~{\rm M}_{\odot}$) is significantly smaller than that of the magnetar.

Provided that the initial velocity of the ejecta of SN 2011kl is $\sim 14,000 \text{ km s}^{-1}$ (the lower limit of the ejecta velocity; see Kann et al. 2016), the inferred values of the initial kinetic energy of this SN is $E_{\rm K,0} \approx$

 2.0×10^{51} erg , indicating that the neutrino-driven mechanism (Janka et al. 2016) is able to provide the $E_{\rm K,0}$ for this SN. But larger velocities require other mechanisms to provide additional $E_{\rm K,0}$.

Furthermore, we used a MCMC method for the G15 and the K16 LCs to constrain the range of the model parameters (we did not perform MCMC for the I16 LC owing to the absence of the error bars); see Table 1. By adopting different values of κ , we found that while the inferred mass is significantly influenced by the values of κ ($M_{\rm ej} = a\kappa^{-1} + b$ (a and b are constants), all other parameters are only slightly affected by the values of κ and no correlation between them and κ has been found.

According to these results, we suggest that the magnetar and the magnetar+⁵⁶Ni models, with or without the cooling effect, can reproduce the LCs of SN 2011kl. ¹¹ In other words, SN 2011kl might be primarily powered by a nascent magnetar.

We thank I. Arcavi for helpful discussions of the cooling model. This work is supported by the National Basic Research Program ("973" Program) of China (grant 2014CB845800) and the National Natural Science Foundation of China (grant 11573014). L.J.W. is supported by the National Program on Key Research and Development Project of China (grant 2016YFA0400801). A.V.F.'s supernova group is supported by the Christopher R. Redlich Fund, the TABASGO Foundation, and the Miller Institute for Basic Research in Science (U.C. Berkeley).

REFERENCES

Arcavi, I., Wolf, W. M., Howell, D. A., et al. 2016, ApJ, 819, 35 Arnett, W. D. 1982, ApJ, 253, 785

Beniamini, P., Giannios, D., & Metzger, B. D. 2017, arXiv:1706.05014

Bersten, M. C., Benvenuto, O. G., Orellana, M., & Nomoto, K. 2016, ApJL, 817, L8

Cano, Z., Johansson A. K. G., & Maeda, K. 2016, MNRAS, 457, 2761

Cano, Z., Wang, S. Q., Dai, Z. G., Wu, X. F. 2017, Advances in Astronomy, 8929054, 1

Cappellaro, E., Mazzali, P. A., Benetti, S., et al. 1997, A&A, 328,

Chatzopoulos, E., Wheeler, J. C., & Vinko, J. 2012, ApJ, 746, 121 Chatzopoulos, E., Wheeler, J. C., Vinko, J., et al. 2013, ApJ, 773,

Chen, K.-J., Moriya, T. J., Woosley, S., Sukhbold, T., Whalen, D. J., Suwa, Y., & Bromm, V. 2017, ApJ, 839, 85

Chen, T.-W., Smartt, S. J., Jerkstrand, A., et al. 2015, MNRAS, 452, 1567

Chevalier, R. A. 1982, ApJ, 258, 790

Chevalier, R. A., & Fransson, C. 1994, ApJ, 420, 268

Chugai, N. N. 2000, Astron. Lett., 26, 797

Chugai, N. N., & Danziger, I. J. 1994, MNRAS, 268, 173

¹⁰ It should be mentioned that the model in which the progenitors have a nonstandard structure (Nakar & Piro 2014; Piro 2015) has been employed to explain some SLSNe whose bolometric LCs exhibit an early-time excess (Smith et al. 2016; Vreeswijk et al. 2017).

2017).

11 We caution that the question of how the magnetar powers an ultralong GRB is still unsolved. Metzger et al. (2015) suggested that a magnetar with $P_0 \approx 2$ ms and $B_p \approx 4 \times 10^{14}$ G can power the ultralong GRB 111209A and SN 2011kl, but Beniamini et al (2017) demonstrated that it is difficult for a magnetar to produce an ultralong GRB. This issue is beyond the scope of this paper and needs additional research. Moreover, we do not attribute the optical afterglow of GRB 111209A to magnetar spin-down emission.

Dai, Z. G., Wang, S. Q., Wang, J. S., Wang, L. J., & Yu, Y. W. ApJ, 817, 132

Dessart, L., Hillier, D. J., Waldman, R., Livne, E., & Blondin, S. 2012, MNRAS, 426, L76

Filippenko, A. V. 1997, ARA&A, 35, 309

Gal-Yam, A. 2012, Science, 337, 927

Gal-Yam, A., Mazzali, P., Ofek, E. O., et al. 2009, Nature, 462, 624

Galama, T. J., Vreeswijk, P. M., van Paradijs, J., et al. 1998, Nature, 395, 670

Gao, H., Lei, W. H., You, Z. Q., & Xie, W. 2016, ApJ, 826, 141
Gendre, B., Stratta, G., Atteia, J. L., et al. 2013, ApJ, 766, 30
Golenetskii, S., Aptekar, R., Mazets, E., et al. 2011, GRB
Coordinates Network, 12663

Gompertz, B. & Fruchter, A. 2017, ApJ, 839, 49

Greiner, J., Mazzali, P. A., Kann, D. A., et al. 2015, Nature, 523, 189

Hjorth, J., & Bloom, J. S. 2012, in Gamma-Ray Bursts, ed. C. Kouveliotou, R. A. M. J. Wijers, & S. E. Woosley (Cambridge Astrophysics Series, Vol. 51; Cambridge Univ. Press), 169

Hjorth, J., Sollerman, J., Møller, P., et al. 2003, Nature, 423, 847 Inserra, C., Smartt, S. J., Jerkstrand, A., et al. 2013, ApJ, 770,

Inserra, C., Smartt, S. J., Gall, E. E. E., et al. 2016, arXiv:1604.01226

Ioka, K., Hotokezaka, K., & Piran, T. 2016, ApJ, 833, 110Iwamoto, K., Mazzali, P. A., Nomoto, K., et al. 1998, Nature, 395, 672

Janka, H.-T., Melson, T., & Summa, A. 2016, ARNPS, 66, 341Kann, D. A., Schady, P., Olivares E., F., et al. 2016, arXiv:1606.06791

Kann, D. A., Schady, P., Olivares E., F., et al. 2017, arXiv:1706.00601

Kasen, D., & Bildsten, L. 2010, ApJ, 717, 245

Kasen, D., Metzger, B. D., & Bildsten, L. 2016, ApJ, 821, 36
Kashiyama, K., Nakauchi, D., Suwa, Y., Yajima, H., & Nakamura, T. 2013, ApJ, 770, 8

- Kotera, K., Phinney, E. S., & Olinto, A. V. 2013, MNRAS, 432, 3228
- Liu, L. D., Wang, L. J., Wang, S. Q., & Dai, Z. G. 2017a, arXiv:1706.01783
- Liu, L. D., Wang, S. Q., Wang, L. J., Dai, Z. G., Yu, H., & Peng, Z. K. 2017b, ApJ, 842, 26
- Liu, Y. Q., Modjaz, M., Bianco, F. B. 2017c, apj, 845, 85
- Lyman, J. D., Bersier, D., James, P. A., Mazzali, P. A., Eldridge, J., Fraser, M., & Pian, E. 2016, MNRAS, 457, 328
- MacFadyen, A. I., & Woosley, S. E. 1999, ApJ, 524, 262
- Maeda, K., Mazzali, P. A., Deng, J., Nomoto, K., Yoshii, Y., Tomita, H., & Kobayashi, Y. 2003, ApJ, 593, 931
- Maeda, K., Tanaka, M., Nomoto, K., Tominaga, N., Kawabata, K., Mazzali, P. A., Umeda, H., Suzuki, T., & Hattori, T. 2007, ApJ, 666, 1069
- Maeda, K., & Tominaga, N. 2009, MNRAS, 394, 1317
- Matheson, T., Filippenko, A. V., Li W., Leonard, D. C., & Shields, J. C., 2001, AJ, 121, 1648
- Mazzali, P. A., Deng, J., Maeda, K., et al. 2002, ApJL, 572, L61 Mazzali, P. A., Deng, J., Nomoto, K., et al. 2006, Nature, 442,
- Mazzali, P. A., Iwamoto, K., & Nomoto, K. 2000, ApJ, 545, 407
 Mazzali, P. A., Kawabata, K. S., Maeda, K., et al. 2005, Science, 308, 1284
- Metzger, B. D., Margalit, B., Kasen, D., & Quataert, E. 2015, MNRAS, 454, 3311
- Moriya, T. J., Chen, T.-W., & Langer, N. 2017, ApJ, 835, 177 Nadyozhin, D. K. 1994, ApJS, 92, 527
- Nagy, A. P. & Vinkó, J. 2016, A&A, 589, 53
- Nakar, E., & Piro, A. L. 2014, ApJ, 788, 193
- Nakauchi, D., Kashiyama, K., Suwa, Y., & Nakamura, T. 2013, ApJ, 778, 67
- Nicholl, M., Guillochon, J., & Berger, E. 2017, arXiv:1706.00825Nicholl, M., Jerkstrand, A., Inserra, C., et al. 2014, MNRAS, 444, 2096
- Nicholl, M., Smartt, S. J., Jerkstrand, A., et al. 2013, Nature, 502, 346
- Nicholl, M., Smartt, S. J., Jerkstrand, A., et al. 2015, MNRAS, 452, 3869
- Nomoto, K., Kobayashi, C., & Tominaga, N. 2013, ARA&A, 51, 457
- Palmer, D. M., Barthelmy, S. D., Baumgartner, W. H., et al. 2011, GRB Coordinates Network, 12640

- Piro, A. L. 2015, ApJL, 808, L51
- Quimby, R. M., Kulkarni, S. R., Kasliwal, M. M., et al. 2011, Nature, 474, 487
- Smith, M., Sullivan, M., D'Andrea, C. B., et al. 2016, ApJL, 818, L8
- Spergel, D. N., Verde, L., Peiris, H. V., et al. 2003, ApJS, 148, 175
 Stanek, K. Z., Matheson, T., Garnavich, P. M., et al. 2003, ApJL, 591, L17
- Stratta, G., Gendre, B., Atteia, J. L., et al. 2013, ApJ, 779, 66
- Taddia, F., Sollerman, J., Leloudas, G., et al. 2015, A&A, 574, 60 Umeda, H., & Nomoto, K. 2008, ApJ, 673, 1014
- Valenti, S., Benetti, S., Cappellaro, E., et al. 2008, MNRAS, 383, 1485
- Valenti, S., Fraser, M., Benetti, S., et al. 2011, MNRAS, 416, 3138Vreeswijk, P. M., Fynbo, J., & Melandri, A. 2011, GCN Circulars, 12648
- Vreeswijk, P. M., Leloudas, G., Gal-Yam, A., et al. 2017, ApJ, 835, 58
- Wang, L. J., Cano, Z., Wang, S. Q., et al. 2017a, arXiv:1702.03156 Wang, L. J., Han, Y. H., Xu, D., et al. 2016a, ApJ, 831, 41
- Wang, L. J., Wang, S. Q., Dai, Z. G., Xu, D., Han, Y. H., Wu, X. F., & Wei, J. Y. 2016b, ApJ, 821, 22
- Wang, L. J., Yu, H., Liu, L. D., Wang, S. Q., Han, Y. H., Xu, D., Dai, Z. G., Qiu, Y. L., & Wei, J. Y. 2017b, ApJ, 837, 128
- Wang, S. Q., Liu, L. D., Dai, Z. G., Wang, L. J., & Wu, X. F. 2016c, ApJ, 828, 87
- Wang, S. Q., Wang, L. J., Dai, Z. G., & Wu, X. F. 2015a, ApJ, 799, 107
- Wang, S. Q., Wang, L. J., Dai, Z. G., & Wu, X. F. 2015b, ApJ, 807, 147
- Wheeler, J. C., Johnson, V., & Clocchiatti, A. 2015, MNRAS, 450, 1295
- Woosley, S. E. 1993, ApJ, 405, 273
- Woosley, S. E. 2010, ApJL, 719, L204
- Woosley, S. E., & Bloom, J. S. 2006, ARA&A, 44, 507
- Yan, L., Lunnan, R., Perley, D., et al. 2017, arXiv:1704.05061
- Yan, L., Quimby, R., Ofek, E., et al. 2015, ApJ, 814, 108 Yu, Y. W., Zhu, J. P., Li, S. Z., Lü, H. J., & Zou, Y. C. 2017,
- ApJ, 840, 12 Zeh, A., Klose, S., & Hartmann, D. H. 2004, ApJ, 609, 952

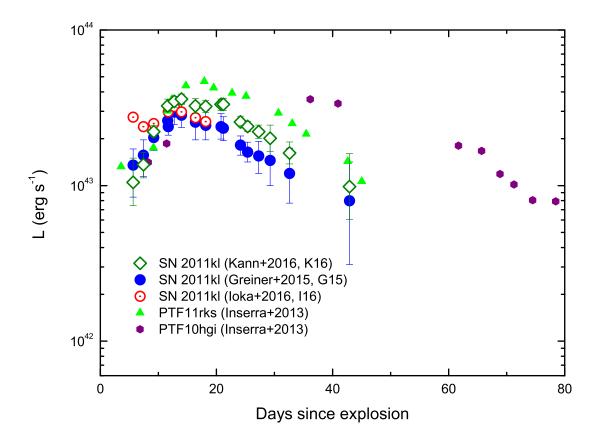


Fig. 1.— LCs of SN 2011kl. The data are taken from Greiner et al. (2015), Ioka et al. (2016), and Kann et al. (2016). For comparison, the early-time ($t \le 80$ days) LCs of SLSNe PTF11rks and PTF10hgi (Inserra et al. 2013) are also shown. The horizontal axis represents the time since the explosion in the rest frame.

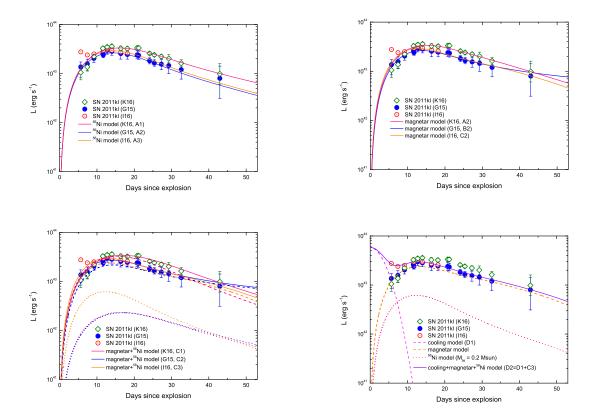


Fig. 2.— The LCs reproduced by different models (A1–A3, B1–B3, C1–C3, and D1–D4) listed in Table 1. Data for SN 2011kl are taken from Greiner et al. (2015), Ioka et al. (2016), and Kann et al. (2016). The thin dotted lines in the lower panels represent the LCs reproduced by 0.1 (the dimmer LCs) or 0.2 $M\odot$ (the brighter LCs) of 56 Ni. The dashed lines in the lower panels represent the LCs reproduced by the magnetar. The horizontal axis represents the time since the explosion in the rest frame.

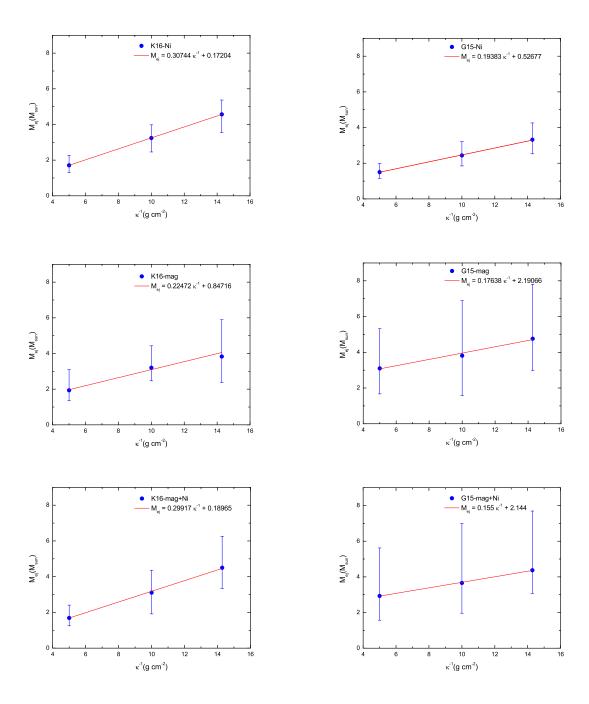


Fig. 3.— Correlation between the ejecta mass and the optical opacity for SN 2011kl.

TABLE 1 Parameters of various models for SN 2011kl. The uncertainties are $1\sigma.$

	$(\text{cm}^2 \text{g}^{-1})$	^M ej (M _☉)	M _{env} (M _☉)	R _{env} (R _☉)	M _{Ni} (M _☉)	$^{B_p}_{(10^{14} \text{ G})}$	P ₀ (ms)	$v_{sc0} (\text{km s}^{-1})$	$(\operatorname{cm}^2\operatorname{g}^{-1})$	$\frac{\kappa_{\gamma,\text{mag}}}{(\text{cm}^2 \text{ g}^{-1})}$	χ^2/dof
⁵⁶ Ni	(cm g)	(IVI _(*))	(W ₁ (•))	(11(.))	(101(*))	(10 G)	(ms)	(KIII S)	(cm g)	(cm g)	
A1(K16ni007)	0.07	$^{4.57}_{-1.03}^{+0.80}$	-	-	$1.42^{+0.04}_{-0.04}$	-	-	$22,905.4^{+3,546.1}_{-4,924.7}$	0.027	-	0.353
A1'(K16ni010)	0.10	$3.24^{+0.74}_{-0.78}$ $1.71^{+0.56}_{-0.40}$	-	-	1.48 + 0.04	-	-	$\begin{array}{c} -4,924.7 \\ 21,710.9 + 4,143.7 \\ -4,636.7 \end{array}$	0.027	-	0.356
A1"(K16ni020)	0.20	$1.71^{+0.56}_{-0.40}$	-	-	$\begin{array}{c} -0.04 \\ +0.06 \\ 1.64 -0.05 \end{array}$	-	-	$19,535.3^{+4,954.4}_{-3,827.8}$	0.027	-	0.360
A2(G15ni007)	0.07	$\begin{array}{c} -0.40 \\ +0.94 \\ 3.32 -0.79 \end{array}$	-	-	0.05 0.05 0.05 0.05	-	-	$\begin{array}{c} -3,827.8 \\ +4,867 \\ 20,387.7 \\ -4,341.8 \end{array}$	0.027	-	0.061
$\mathrm{A2'}(\mathrm{G15ni010})$	0.10	$\begin{array}{c} 0.02 - 0.79 \\ -0.77 \\ 2.44 - 0.59 \end{array}$	-	-	$\begin{array}{c} -0.05 \\ +0.06 \\ 1.11 \\ -0.05 \end{array}$	-	-	$19,868.6^{+4,999.6}_{-4,066.9}$	0.027	-	0.062
A2" (G15ni020)	0.20	$1.50^{+0.48}_{-0.35}$	-	-	$\begin{array}{c} -0.05 \\ +0.07 \\ 1.25 -0.06 \end{array}$	-	-	$19,993.7 + 4,941.9 \\ -3,723.3$	0.027	-	0.092
A3(I16ni007)	0.07	2.12	-	-	1.1	-	-	21,000	0.027	-	-
magnetar											
B1(K16mag007)	0.07	$3.83^{+2.06}_{-1.46}$			0	$5.99^{+1.75}_{-5.55}$	$10.83^{+0.49}_{-6.94}$	$21,715.3^{+4,293.1}_{-4.973.8}$		$1,918.79^{+5,486.67}_{-1.918.775}$	0.259
B1(K16mag010)	0.10	$_{2.20}+1.23$	-	-	0	a aa+1.37	$ \begin{array}{r} -6.94 \\ -94 \\ -3.35 \end{array} $	21, 113.3 - 4,973.8 $21, 159.4 + 4,768.8$ $-4,045.1$	-	$1,918.79 = 1,918.775 \\ +3,728.79 \\ 4,426.31 = 3,564.503$	0.398
B1''(K16mag020)	0.10	$\begin{array}{c} 3.20 - 0.73 \\ -0.73 \\ 1.94 - 0.58 \end{array}$	-	-	0	6.62 - 2.15 $6.75 + 1.35$ -1.38	$\begin{array}{r} -3.35 \\ -3.30 \\ 11.08 -0.61 \end{array}$	21, 159.4 - 4,045.1 $20, 672.7 + 4,445.9$ $-4,609.8$	-	4,420.31 - 3,564.503 $2,781.08 + 4,888.58$ $-2.781.0756$	0.361
, – ,		$\begin{array}{c} 1.94 - 0.58 \\ -0.58 \\ 4.76 - 1.78 \end{array}$	-	-		$9.72^{+3.23}_{-4.13}$	11.08 - 0.61 $12.07 + 1.15$ $12.07 - 2.52$	20,872.7 - 4,609.8 20,846.3 + 3,887.4 20,846.3 - 4,860.9	-	2, 781.08 - 2,781.0756 4, 478.71 - 3,969.36	
B2(G15mag007)	0.07	$^{4.76}_{-1.78}$	-	-	0	9.72 - 4.13	12.07 - 2.52	$20,846.3_{-4,860.9}$ $21,517.1_{-4,610.3}^{+4,308.8}$	-	4,478.71 - 3,969.36 $2,559.96 + 4,995.82$ $2,559.96 - 2,559.941$	0.065
B2'(G15mag010)	0.10	$3.81^{+3.08}_{-2.23}_{\pm 2.22}$	-	-	0	$9.40^{+4.68}_{-8.14}$	$10.01^{+2.89}_{-4.74}$	21,517.1 - 4,610.3	-	2,559.96 - 2,559.941 $3,855.41 + 4,101.43$ $3,855.41 - 3,764.804$	0.066
B2"(G15mag020)	0.20	$3.10^{+2.22}_{-1.43}$	-	-	0	$12.20^{+4.80}_{-3.97}$	$9.26^{+3.41}_{-3.35}$	$20,798.6^{+5,404.0}_{-5,027.5}$	-		0.066
B3(I16mag007)	0.07	2.12	-	-	0	6.5	13.2	21,000	-	104	-
magnetar $+^{56}$ Ni											
C1(K16magni007)	0.07	$4.50^{+1.76}_{-1.16}$	-	-	$0.11^{+0.06}_{-0.07}$	$6.94^{+1.51}_{-1.62}$	$11.46^{+0.46}_{-0.79}$	$21,763.4^{+4,440.2}_{-4,977.1}$	0.027	$4,229.65^{+3,885.96}_{-3,633.31}$	0.409
C1'(K16magni010)	0.10	$3.11^{+1.25}$	-	-	$0.11^{+0.06}$	$6.80^{+1.58}_{-1.85}$	$11.3^{+0.46}_{-1.01}$	20, 334, 9 + 5, 272.6	0.027	4.040.85+3,948.94	0.413
C1"(K16magni020)	0.20	$1.69^{+0.72}$	-	-	$0.11^{+0.05}$	$7.12^{+1.28}_{-1.43}$	$11.41^{+0.41}$	21,537.6 + 5,034.7	0.027	3993.19 +4,038.74	0.406
C2(G15magni007)	0.07	4 37+3.32	-	-	0.10 + 0.06	10.07 + 3.93		19 410 8+5,156.7	0.027	3. 670.59 +4,243.63	0.071
C2'(G15magni010)	0.10	$3.66^{+3.33}_{-1.70}$	-	-	$0.11^{+0.05}_{-0.07}$	$ \begin{array}{r} -7.30 \\ -7.30 \\ -9.10 \end{array} $	$12.21^{+1.65}_{-3.60}$ $10.80^{+2.83}_{-5.95}$	21.051.0 + 4,496.1	0.027	2,767.03+4,768.41	0.071
C2"(G15magni020)	0.20	$2.93^{+2.69}_{-1.36}$	-	-	$0.10^{+0.07}_{-0.07}$	$14.10^{+5.12}_{-4.33}$	$10.47^{+2.87}_{-5.62}$	$20,857.9 \begin{array}{r} -4,415.6 \\ +4,792.0 \\ -4,538.1 \end{array}$	0.027	5007.93 + 3334.9 -3376.97	0.069
C3(I16magni007)	0.07	2.12	-	-	0.2	6.5	14.2	21,000	0.027	0.13	-
magnetar+ ⁵⁶ Ni											
+cooling											
D1 (I16cooling)	0.07	2.12	0.63	51.4	0	-		21,000		-	-
D2(I16magnicooling) ^a D2'(I16magnicooling) ^a	0.07 0.07	2.12 1.6	0.63 0.45	51.4 103	0.2	6.5 6.5	14.2 14.2	21,000 16,000	0.027 0.027	0.13 0.13	-
D2 (110magnicooning)	0.01	1.0	0.40	103	0.2	0.0	14.4	10,000	0.041	0.13	

 $[^]a$ The cooling+magnetar+ 56 Ni model (D2 = D1 + C3).